The Pennsylvania State University

The Graduate School

Department of Mechanical and Nuclear Engineering

MODIFICATIONS TO THE RUNNER BLADE TO IMPROVE OFF-DESIGN EFFICIENCIES OF HYDRAULIC TURBINES

A Thesis in

Mechanical Engineering

by

Matthew D. Erdman

Submitted in Partial Fulfillment
of the Requirements
for the Degree of

Master's of Science

May 2016

The thesis of Matthew D. Erdman was reviewed and approved* by the following:

John M. Cimbala
Professor of Mechanical Engineering
Thesis Advisor

Savas Yavuzkurt
Professor of Mechanical Engineering

Karen Thole
Professor of Mechanical Engineering
Head of the Department of Mechanical and Nuclear Engineering

*Signatures are on file in the Graduate School

ABSTRACT

Hydroturbines are known to have very high efficiency at their best efficiency point (BEP). However, it has become increasing beneficial to run some hydroturbines at conditions that are significantly different than BEP. This is a direct result of volatile price fluctuations on the electric market, limited storage capabilities, and environmental rules and regulations. Running the hydroturbine at off-design conditions can result in a significant amount of residual swirl in the draft tube. The presence of this residual swirl is particularly detrimental to the performance of Francis hydroturbines since they rely on a pressure head to generate power.

Previous research at The Pennsylvania State University numerically discovered that injecting water through the trailing edge of the wicket gates could change the bulk flow direction upstream of the runner blades. In this manner, the flow rate and swirl angle entering the runner blade could be altered to limit residual swirl in the draft tube. The research determined that properly tuned jets could result in a significant improvement in turbine efficiency when the hydroturbine was operating at low flow. However, this required pumping water through channels into a region of relatively high pressure. This pump requirement lessened the effectiveness of the wicket gate trailing edge injection.

The concept of water jet injection was further explored in the present work. However, instead of injecting water into a region of relatively high pressure, water jets were placed at the trailing edge of the runner blades where there is a region of relatively low pressure. It was determined that, although this water jet injection improved the off-design efficiency of a low flow case by 0.8%, the hydroturbine now required a larger head in order to maintain the flow rate. The present work found no increase in efficiency for the high flow case with the added water jet injection technique.

TABLE OF CONTENTS

LIST OF FIGURES

LIST OF TABLES

LIST OF SYMBOLS

$\dot{W}_{ideal}$	Maximum power that can be extracted from the hydroturbine
ρ	Density of the fluid (water in the present study)
g	Acceleration due to gravity
Q	Volume flow rate through the hydroturbine
H_{gross}	Maximum difference in height from the top of the reservoir to the tailrace
H	Net head through the hydroturbine
EGL	Energy Grade Line
P	Local Pressure
v	Magnitude of the local velocity
z	Reference height
Φ	Total surface flux
ϕ	Cell face flux
ψ	Non-dimensional head coefficient
φ	Non-dimensional flow coefficient
Ω	Angular velocity of the runner blades
R_{ref}	Reference radius of the runner blades
η	Efficiency of the hydroturbine
T	Torque produced by the hydroturbine
W	Relative velocity of fluid at the trailing edge of the runner blades
U	Tip velocity of fluid at the trailing edge of the runner blades
V	Absolute velocity of fluid at the trailing edge of the runner blades
N_{St}	Specific speed of the hydroturbine

ACKNOWLEDGMENTS

There are many people who have assisted my journey to where I am today. First, I would like to thank Penn State University for the opportunity to study as well conduct this research. Furthermore, I would like to thank Bryan Lewis, whose prior research and insight provided the basis for the present work. I would also like to thank Alex Wouden for his willingness to continually offer insight as the project developed. Finally, I would like to express extreme gratitude to my advisor, John Cimbala, for his continued support and guidance. His patience, honesty, and dedicated work has enabled me to not only grow as an engineer but as a person.

The information, data, or work presented herein was funded in part by the Office of Energy Efficiency and Renewable Energy (EERE), U.S. Department of Energy, under Award Number DE-EE0002668 and the Hydro Research Foundation.

Chapter 1

Introduction

There are numerous reasons that a hydroturbine may be run at conditions differing from its design point (the best efficiency point or BEP). For instance, price fluctuations on the electric market, limited storage capabilities, and environmental rules and regulations often require hydroturbines to be run over a range of conditions. When operated at these partial load conditions, the draft tube can have large amounts of residual swirl. This residual swirl has been linked to the formation of a large helical vortex more commonly known as "vortex rope." The vortex rope is now known to be a significant contributor to the instabilities as well as loss of efficiency that result during operation at off-design conditions. The residual swirl causes a significant head loss that is specifically relevant in reaction turbines (such as Francis Turbines) which draw power directly from the pressure head.

Given the detrimental effect of residual swirl in the draft tube, further analysis and investigation are needed into methods that limit or eliminate that swirl. This research study will investigate one such method using computer simulations. Therefore, the present work serves to investigate methods to increase the turbine efficiencies under various operating conditions and develop simulations for optimizing the operation of hydroturbines.

Hydroturbine Operation and Performance

Figure 1-1 illustrates the standard set-up for a hydroelectric plant [1]. The Pitot tubes are shown for illustration only. For any plant, the maximum power $\dot{W}_{ideal}$ that can be extracted from a hydroturbine is defined as

$$\dot{W}_{ideal} = \rho g Q H_{gross} \tag{1.1}$$

Where ρ is the density of the fluid, g is acceleration due to gravity, Q is the volume flow rate (often written as $\dot{V}$), and H_{gross} is the maximum difference in height from the top of the reservoir to the tailrace.

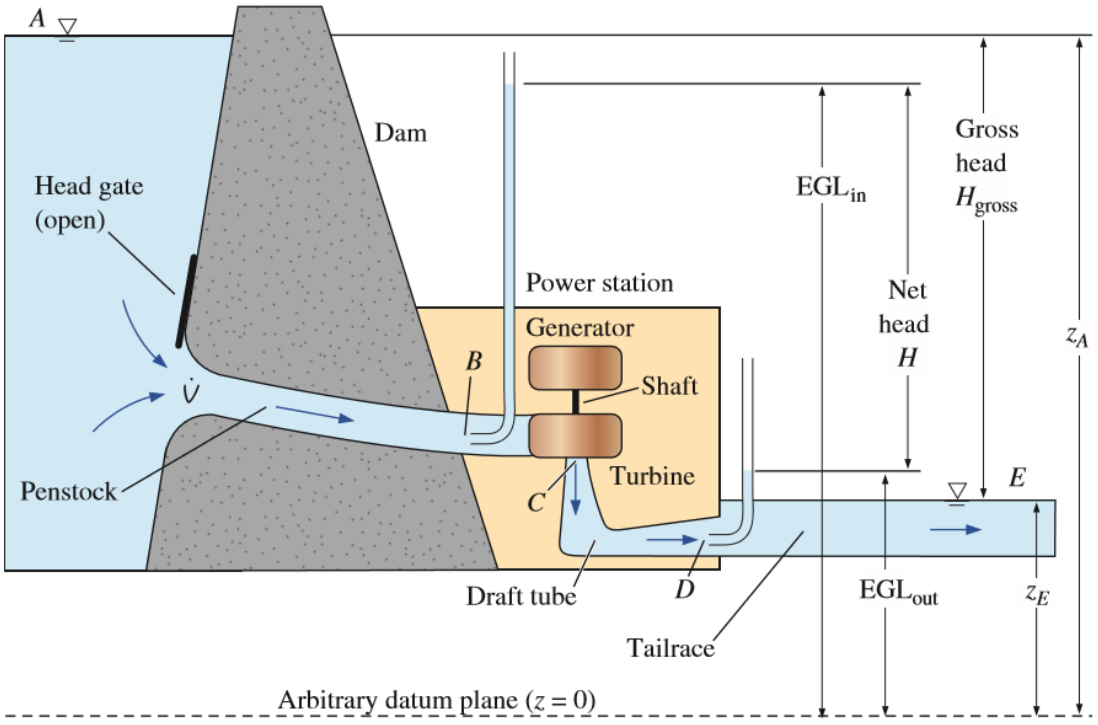

Figure 1-1. Standard set-up for a Francis hydroturbine in a hydroelectric plant. Not drawn to scale. [1]

However, there are losses throughout the hydroelectric plant such as in the penstock and tailrace. Since hydroturbine manufacturers are concerned with the head that the turbine itself sees, the net head neglects the losses in the penstock and tailrace and defines the net head, H, as

$$H = EGL_{in} - EGL_{out} \tag{1.2}$$

where EGL_{in} is defined immediately before the turbine and EGL_{out} is defined at the exit of the draft tube because the draft tube is considered to be vital to the turbine operation. The energy grade line (*EGL*) is defined as the sum of the pressure, velocity, and elevation heads

$$EGL = \frac{P}{\rho g} + \frac{V^2}{2g} + z \tag{1.3}$$

where P is the local pressure, V is the magnitude of the local velocity, and z is the reference height. Similarly, the computational net head is define as the numerically integrated change in EGL. This is possible because the average pressure and velocity are known for each computational cell. Thus, the net head is

$$H = \frac{1}{\rho \Phi_{in}} \sum_{in} \rho \phi \left(\frac{P}{\rho g} + \frac{V^2}{2g} + z \right) - \frac{1}{\rho \Phi_{out}} \sum_{out} \rho \phi \left(\frac{P}{\rho g} + \frac{V^2}{2g} + z \right) \tag{1.4}$$

where ϕ is the cell face flux and Φ is the total surface flux.

Hydroturbine performance is often characterized with the use of non-dimensional turbine coefficients. The formal definition of these coefficients may vary if the author chooses different scaling constants; however, this paper uses the definitions provided by Nilsson and Dividson in order to maintain consistency [2]. The relevant coefficients for the present work are as follows

$$\psi = \textit{Head Coefficient} = \frac{2gH}{\Omega^2 R_{ref}^2} \tag{1.6}$$

$$\varphi = \textit{Flow Coefficient} = \frac{Q}{\pi \Omega R_{ref}^3} \tag{1.7}$$

Additionally, the efficiency of the hydroturbine is defined as the ratio of the power output of the turbine to the available energy in the fluid. Thus,

$$\eta = \frac{\dot{W}}{pgQH} \tag{1.9}$$

It should be noted that

$$\dot{W} = \Omega T \tag{1.10}$$

for this flow. Isocontours of efficiency as a function of φ and ψ, commonly referred to as a "hill chart" are often provided for a given turbine. The operational hill chart for the GAMM Francis Turbine is provided in Figure 2-2.

Vortex Rope Formation

The draft tube was first patented in 1840 [3]. By attaching a diffuser after the turbine blades, the turbine wheel could be placed above the tailrace without a loss of head. This reduced construction costs and significantly decreased the difficulty of maintenance. However, when the turbine operates at off-design conditions, residual swirl in the draft tube can lead to the formation of a vortex rope. The unsteady swirling flow creates a large recirculation region near the center of the draft tube that is filled with slowly moving fluid. Since the diffusor relies on this fluid's velocity to regain the kinetic energy of the discharging water, the presence of the slowly moving fluid associated with the vortex rope results in a substantial reduction in efficiency. Moreover, cavitation can occur if the local pressure in the vortex rope is below the liquid vapor pressure. Cavitation has the potential to severely damage the turbine and shorten its life expectancy. For this reason, a vortex rope, such as the one pictured in Figure 1-2, is extremely undesirable. The present work therefore attempts to eliminate or impede its development.

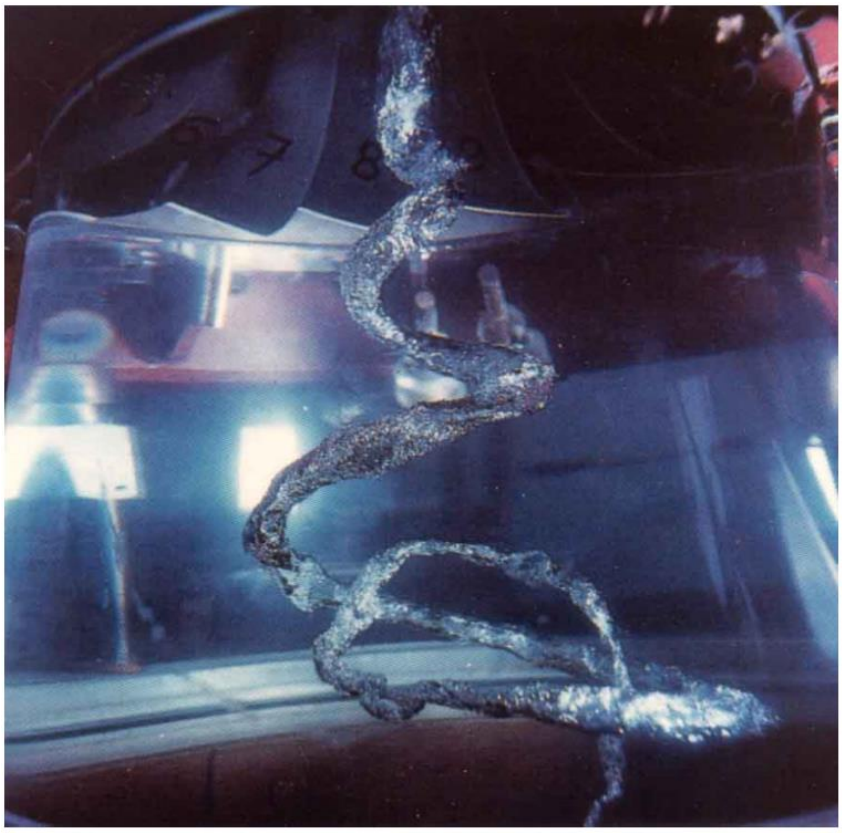

Figure 1-2. Cavitating vortex rope in a Francis turbine model test. [4]

Velocity diagrams can best illustrate the predicted operation of the hydroturbine. In Figure 1-3, W represents the relative velocity and U represents the tip velocity of the blade. When these vectors are combined, the resultant vector is the absolute velocity V. At BEP, the absolute velocity should be perpendicular to the tip velocity. This corresponds to no tangential flow in the draft tube, meaning that no vortex rope should be present. Figure 1-3a shows the velocity diagram of a turbine blade at BEP. However, if the turbine is operating in a low flow environment, the relative velocity of the flow is too small to account for the tip velocity (which remains unchanged). Thus, the absolute velocity has a component in the tangential direction (parallel to the tip velocity) as seen in Figure 1-3b. The larger the tangential velocity the more swirl present exiting the draft tube. Conversely, when the turbine is operating in a high flow environment, the

relative velocity is too large and results in a tangential absolute velocity component in the opposite direction (Figure 1-3c). Since it has been shown that the tangential velocity results in decreased efficiencies due in part to the presence of a vortex rope, the present work aims to turn the flow to decrease the magnitude of this tangential velocity

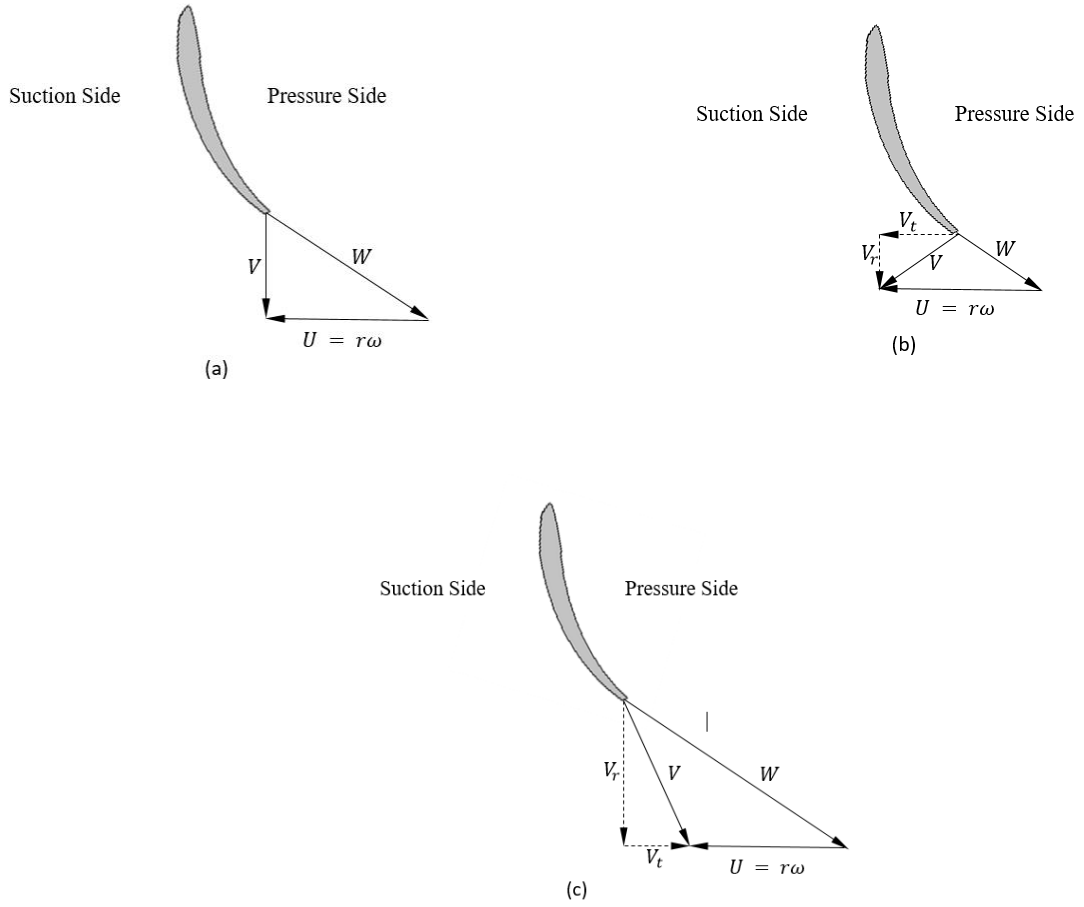

Figure 1-3. Runner blade velocity diagrams for (a) BEP, (b) low flow, and (c) high flow conditions.

Chapter 2

Description of GAMM Francis Turbine

The GAMM Francis Turbine model used in the present work was designed and tested by the IMH-IMHEF-EPFL water turbine laboratory in Lausanne, Switzerland. This model was chosen as its geometry, performance and flow surveys were made public in the 1989 GAMM Workshop on 3-D Computation of Incompressible Internal Flows [5]. Turbine geometry and performance measurements are typically well guarded secrets in the hydroturbine industry. Thus, despite several known problems in the GAMM Francis Turbine model, it is be the main focus of the present analysis as it is the only publically available Francis turbine model.

The GAMM Turbine model discussed above has a specific speed of N_{St} = 0.5, a reference runner radius of R_{ref} = 0.2 m, and a rotation speed of 52.36 rad/s (500 RPM). It should be noted that this is significantly smaller than any operational full-scale Francis turbines due to the difficulties of experimentally testing full-size models. The flow parameters were surveyed using 6 mm diameter five-hole pressure probes [5] and published according to the diagram in Figure 2-1. Unfortunately, the measured velocity profiles were too close to the turbine blades for accurate computational modeling. For this reason, the velocities were extrapolated upstream in the manner discussed in the *Computational Methods* section. The GAMM conference proceedings also provided a hill chart which was modified by Nilsson and Davidson [2] for the operational performance of the GAMM Francis turbine. The velocity profiles were measured for five different operational conditions. The present work examines the model at the first 3 survey locations (labeled 1, 2 and 3 in Figure 2-2) which are BEP, low flow, and high flow operating conditions, respectively. The coefficients of these operating conditions are summarized in Table 2-1.

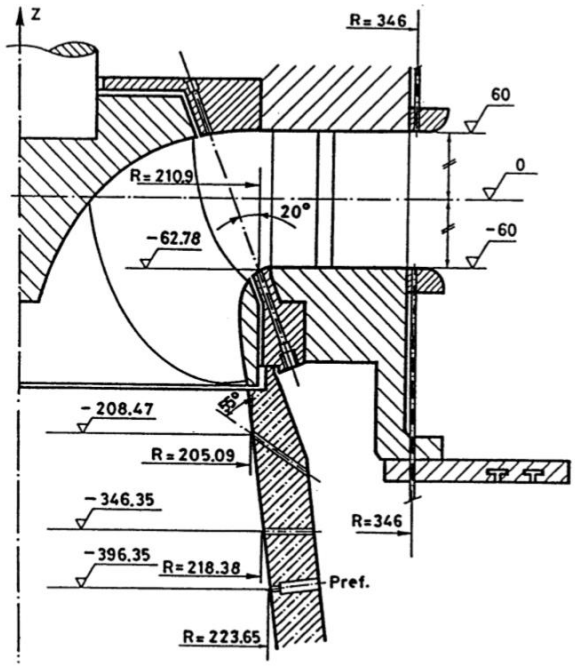

Figure 2-1. Meridonal profile of the GAMM turbine showing the flow survey locations. (units in mm) [5].

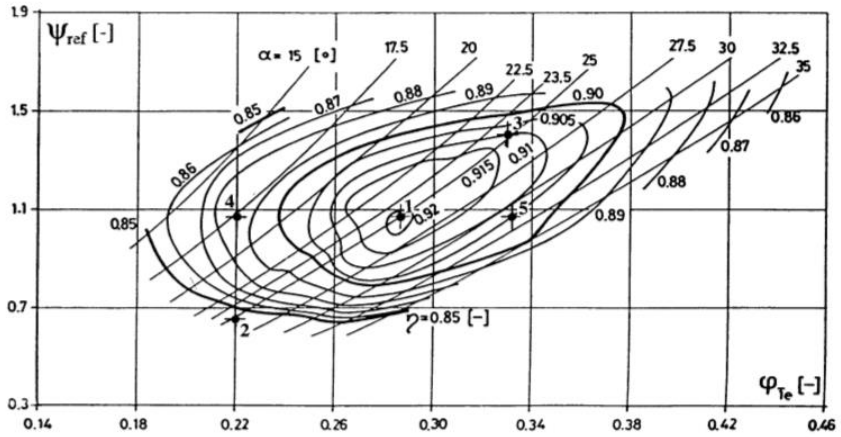

Figure 2-2. Operational hill chart for the GAMM Francis Turbine model as a function of Flow Coefficient $\varphi = \frac{Q}{\pi \Omega R_{ref}^3}$ and Head Coefficient $\psi = \frac{2gH}{\Omega^2 R_{ref}^2}$ [2]

Table 2-1. Various operating conditions of the GAMM Francis Turbine model [5]

Operating Condition	Flow Coefficient φ	Head Coefficient ψ
1	0.286	1.07
2	0.220	0.66
3	0.330	1.40

Chapter 3

Design of Runner Blade Trailing Edges

Lewis [3] previously determined that the bulk mean flow could be altered upstream of the turbine using the combination of a beveled trailing edge and water jet injection. The final design of the trailing edge geometry of Lewis's modified wicket gate is shown in Figure 3-1. Lewis used a Taguchi design method to alter the jet position and angle to determine the optimal configuration that produced the maximum change in flow angle [3]. For the geometry given in Figure 3-1, Lewis discovered that water jet injection from Jet 1 would turn the bulk mean flow upwards and water jet injection from Jet 2 would turn the bulk mean flow downwards.

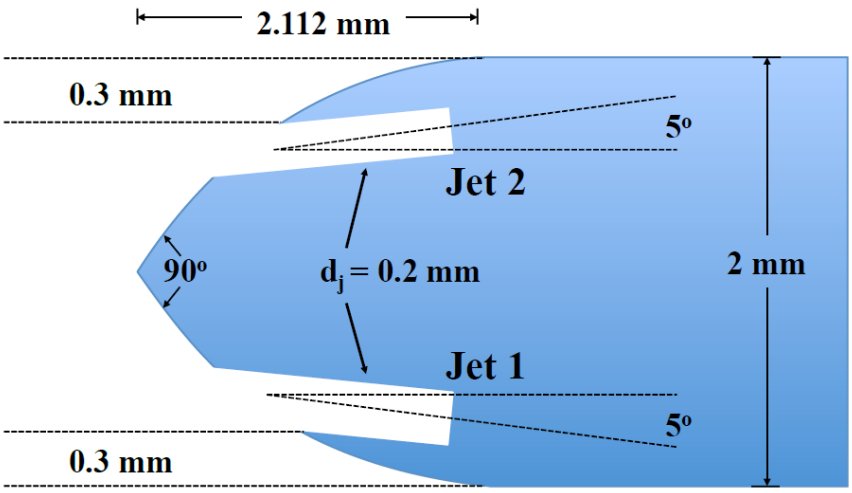

Figure 3-1. Final design of the trailing edge geometry added to the wicket gates of the GAMM Francis turbine by Lewis [3].

Since Lewis determined that the above configuration produced the maximum change in swirl angle, the above configuration was scaled on the basis of trailing edge thickness for application to

the runner blades. Runner blade trailing edge modification proved more complicated than wicket gate modification for two reasons. Firstly, the wicket gate trailing edge had a constant thickness of 2 mm while the runner blade trailing edge thickness varies from 1.458 mm to 2.241 mm. For this reason, most of the dimensions of the beveled trailing edge are scaled with the thickness. The exception is the thickness of the water jets themselves, which is scaled based on the average trailing edge thickness and kept constant for the entire span of the trailing edge to ensure a constant water jet flow rate along the trailing edge. The beveled edge geometry has been provided at two locations (the top and bottom of the trailing edge) in Figure 3-2. The second change from the wicket gate modification results from the uneven shape of the original blunt trailing edge. In order to allow for a smooth transition from the blade to the beveled edge, minor tangential extensions were added to bridge the gap between the original blunt edge and the beveled edge. It should be noted that the thickness of the blade at the end of these extensions is the thickness that is utilized when carrying out the scaling of the beveled edge instead of using the original trailing edge thickness.

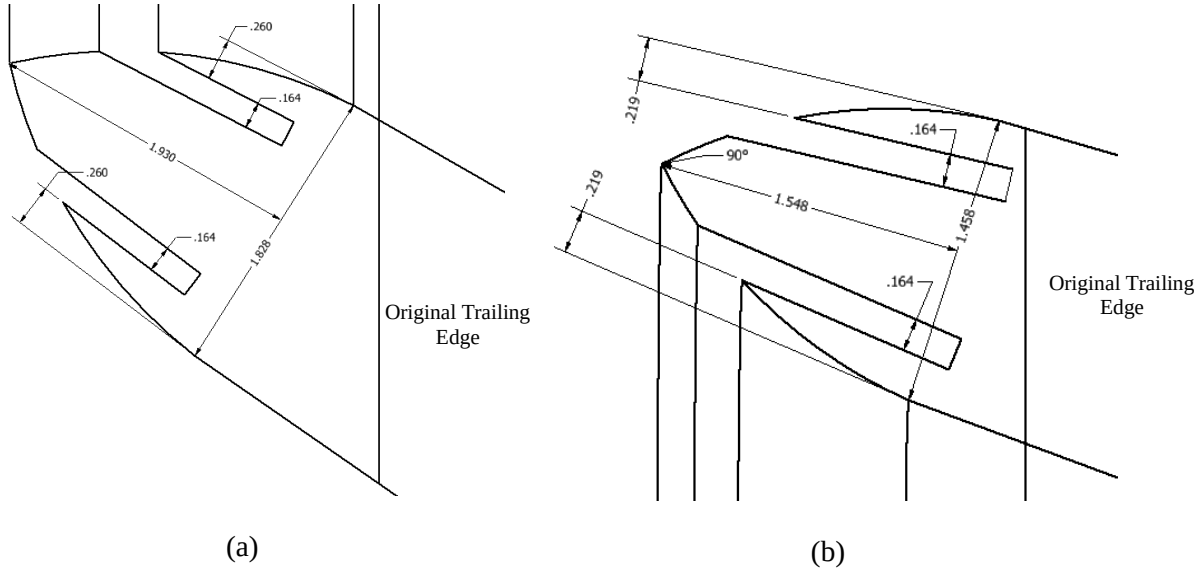

Figure 3-2. Upper (a) and lower (b) runner blade trailing edge modifications.

Chapter 4

Computational Methods

The computational model was run as a steady-state simulation in ANSYS-Fluent. In order to minimize the number of cells, a periodic solution for one of the thirteen blades was solved instead of a full-wheel simulation. Due to the stiffness of the computations, first order discretization methods were initially used. Once the model began to converge with more stability, second-order upwinding was the discretization method for all variables of interest except pressure, for which second order was the option chosen. Due to excessive skewness in the region surrounding the trailing edge, the under-relaxation factors as well as residuals were set extremely low. The loss in speed of computation was made up for in the stability of the solution. A standard realizable k-ε model was used with enhanced wall functions employed in order to effectively model the turbulent properties near the wall. The swirling nature of the flow in the draft tube has the potential to cause backflow in the model. For this reason, a frictionless body of length equal to the entire domain was added to the exit of the draft tube.

As was mentioned in Chapter 2, the model velocity profiles were surveyed very close to the runner blades themselves. These velocity profiles were extrapolated upstream to a radial location of 239.3 mm to ensure that the computational inlet was not affected by the runner blades themselves. The magnitude of the radial and axial velocity was set as the radial inlet velocity and scaled to achieve the same flow rate upstream, while the tangential velocity was extrapolated upstream using conservation of angular momentum. The axial velocity at the new inlet was fixed to zero. This approach was used both by Lewis [3] and Nilsson and Davidson [2]. Additionally, the portion of the draft tube before the bend was used in the computational domain in the same

manner as Lewis [3]. Figure 4-1 shows the computational domain (dashed lines) used in the present work that has been extrapolated from the survey locations (dotted lines).

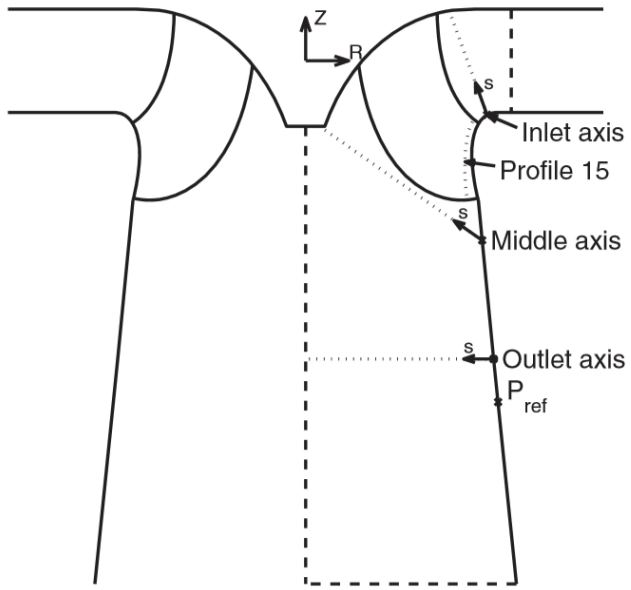

Figure 4-1. Computational domain extrapolated from survey locations [3]

A quick mesh independence study was performed for BEP conditions. Although the fine mesh produced slightly more accurate results, Table 4-1 shows that both the course mesh (2.82 million cells) and fine mesh (3.67 million cells) produced results in line with experimental or computational results. Both meshes have a significantly larger number of cells compared to that of Lewis or Nilsson and Davidson. However, a large portion of the cells were clustered around the trailing edge of the runner blade in order to achieve the necessary resolution for the injection of the water jets. Since neither previous investigation had water jet injection in this domain, it is understandable that they were able to accomplish the computation with significantly fewer cells. An additional consequence of the increased cell count is observed in that the coarse mesh in this

study was even more accurate in determining the torque, head and efficiency than either computational study completed by Lewis [3] or Nilsson and Davidson [2].

The results were calculated for each of the 3 flow conditions and compiled into Tables 4-1, 4-2, and 4-3. Both the BEP and high flow simulations matched the experimental and computational results. However, for the low flow case, the efficiency varied slightly from the experimental results despite matching the other published computational results. This computational error could be due to the lack of resolution near the cone of the draft tube where the unsteady vortex rope would be forming. Nonetheless, since the present work aims to show the change that occurs with water jet injection, slight differences with experimental results are irrelevant. The variation of the performance variables with and without injection is the main objective.

Table 4-1. Comparison of the Experimental and Computed head, H, torque T and efficiency η for the BEP conditions

Data Source	H (m)	T (Nm)	η (%)
Experimental	5.98	388	92.0
Nilsson and Davidson [2]	6.18	413	95.8
Lewis Fine Grid [3]	6.08	400	94.3
Course Grid	6.07	397	94.1
Fine Grid	6.02	390	93.0

Table 4-2. Comparison of the Experimental and Computed head, H, torque T and efficiency η for the low flow conditions

Data Source	H (m)	T (Nm)	η (%)
Experimental	3.69	170	85.0
Nilsson and Davidson [2]	3.73	191	94.8
Lewis Fine Grid [3]	3.69	180	90.0
Fine Grid	3.88	188	89.5

Table 4-3. Comparison of the Experimental and Computed head, H, torque T and efficiency η for the high flow conditions

Data Source	H (m)	T (Nm)	η (%)
Experimental	7.83	579	91.0
Nilsson and Davidson [2]	8.29	625	92.1
Lewis Fine Grid [3]	8.09	603	91.7
Fine Grid	8.11	599	90.9

Chapter 5

Performance Evaluation of GAMM Francis Turbine

The model was then simulated for the various flow conditions in conjunction with water jet injection. The water jet velocities were scaled in order to contribute a volume flow rate equal to one, two, or three percent of the main flow. For convention, Jet 1 is the water jet on the pressure side of runner blade and Jet 2 is on the suction side of the runner blade. Recall that Figure 1-3 demonstrates that, for the low flow condition, there is a component of tangential velocity in the direction of the tip velocity. In order to cancel out that component, the mean bulk flow must be turned in the opposite direction. This requires that Jet 2 on the suction side must be used, as discussed in *Chapter 3*. Conversely, the high flow case requires that the mean bulk flow must be turned in the direction of the tip velocity and should require the activation of Jet 1. The computed head, torque, and efficiency for each case were calculated and sorted into Tables 5-1 and 5-2. Initially for the high flow case, Jet 1 was activated to turn the bulk mean flow as discussed above. Surprisingly, this resulted in a lower torque and water jet injection from Jet 2, which was the wrong jet in order to correctly change flow direction, resulted in a higher torque. However, Jet 1 was accompanied with a larger increase in required head such that the overall efficiency decreased. Likewise, Jet 2 did have a small decrease in required head but the relatively larger loss in torque resulted in a decrease in efficiency. Therefore, the water jet injection modification failed to produce an increase in efficiency for the high flow case. However, Figures 5-2 through 5-6 do demonstrate that the flow was altered in the originally anticipated manner for the high flow case.

Table 5-1. Comparison of the computed head, H, torque T and efficiency η for the high flow conditions with various types of blowing

Data Source	H (m)	T (Nm)	η (%)
No blowing	8.11	599	90.9
1% Jet 1 Blowing	7.97	586	90.5
2% Jet 1 Blowing	7.53	548	89.6
2% Jet 2 Blowing	8.81	647	90.5
3% Jet 2 Blowing	9.21	673	90.0

In order to analyze the effect of the water jet injection technique on the flow, it is necessary to define a constant view plane for observing the plane. Figure 5-1 displays this chosen view for the virtual full wheel (Figure 5-1a) and a single blade (Figure 5-1b). Since these images are taken from the same view, in can be seen that the single blade is rotating in the same counterclockwise manner that the full wheel in (Figure 5-1a) would be.

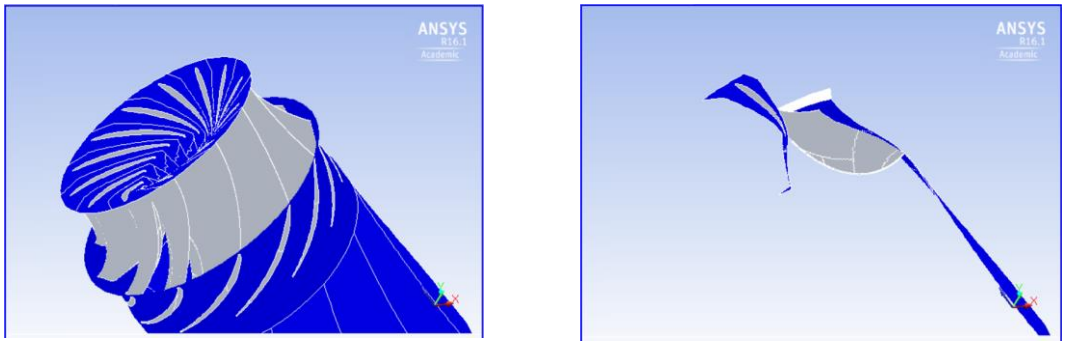

(a) (b)

Figure 4-1. Crown, runner blades, band and draft tube for full wheel (a) and a chosen single blade (b) from the chosen view.

Now that a consistent view has been defined, the tangential velocity through threes slices of the computational domain can be examined for various jet flow conditions. As discussed above, the high flow case should have residual tangential velocity in the direction opposite of the tip velocity, which corresponds to a negative tangential velocity for counterclockwise runner blade rotation. Figure 5-2 shows that the tangential velocities after the trailing edge for the top, middle,

and bottom slices of the runner blade are slightly negative as expected. Likewise, Figures 5-3 and 5-4 demonstrate the Jet 2 activation results in an increased magnitude of this negative tangential velocity, which is exactly what is not desired but is the expected result. As discussed, Jet 2 resides on the suction side on the blade and thus turns the flow in the direction opposite the tip velocity, contributing to a larger residual swirl. Conversely, Jet 1 activation should work to cancel out the residual swirl. Figures 5-5 and 5-6 demonstrate that the Jet 1 activation does result in a lessened tangential velocity. This can especially be seen in the contour plot nearest to the bottom of the runner blade.

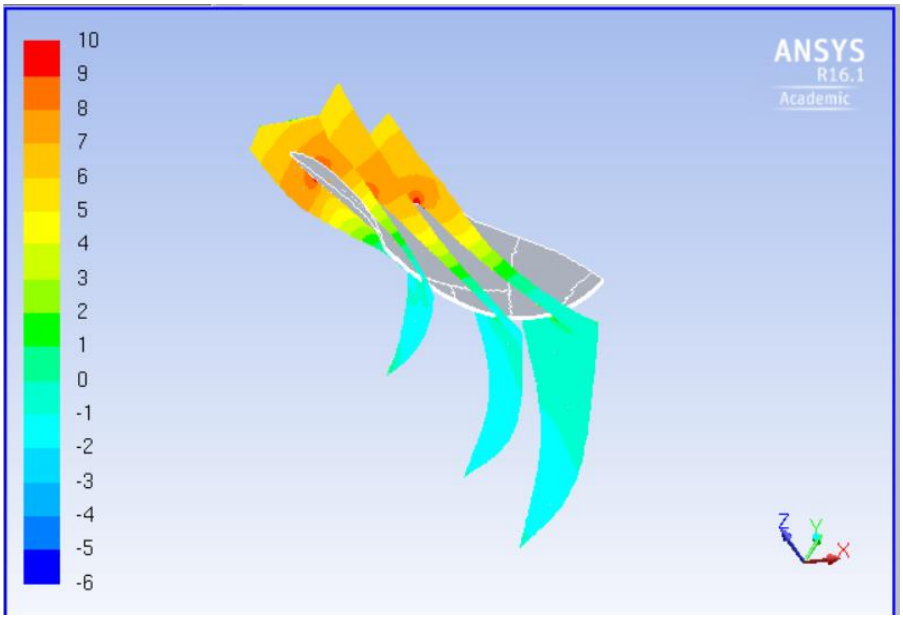

Figure 5-2. Contours of tangential velocity (m/s) for a single Francis GAMM runner blade under high flow conditions with no water jet activation.

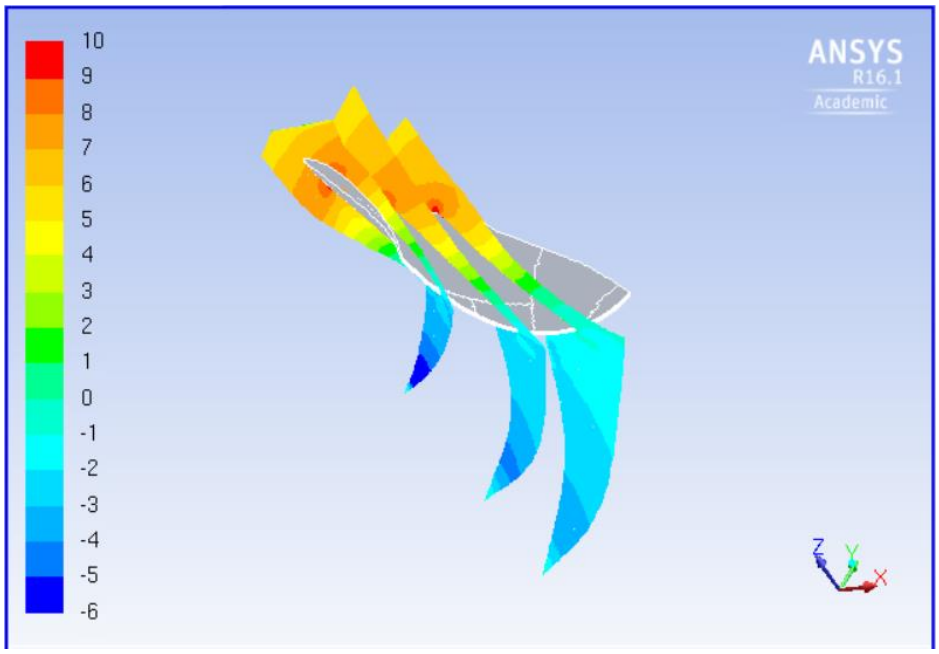

Figure 5-3. Contours of tangential velocity (m/s) for a single Francis GAMM runner blade under high flow conditions with jet 2 injection of 2% volume flow rate.

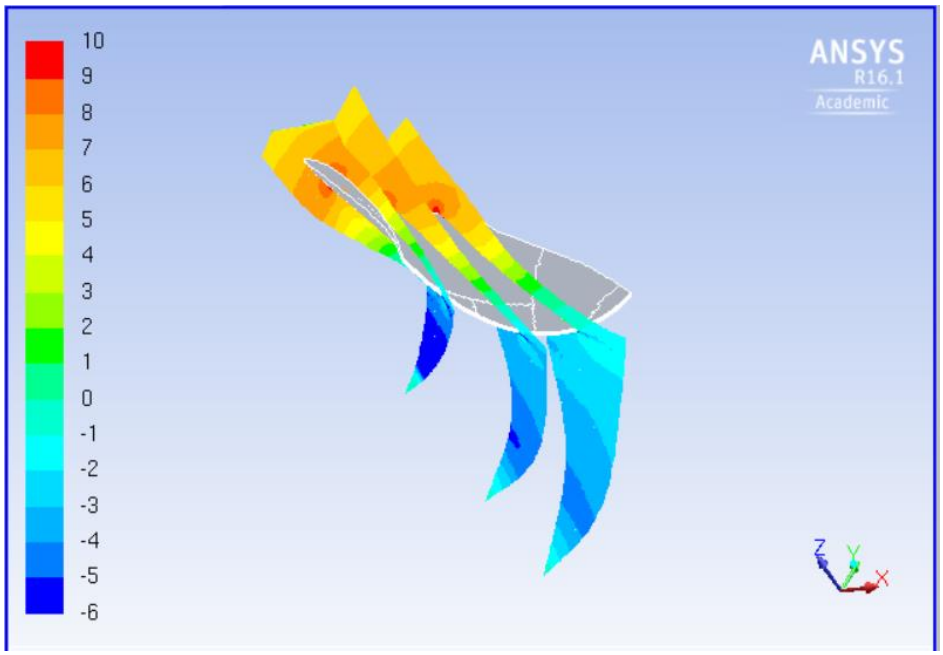

Figure 5-4. Contours of tangential velocity (m/s) for a single Francis GAMM runner blade under high flow conditions with jet 2 injection of 3% volume flow rate.

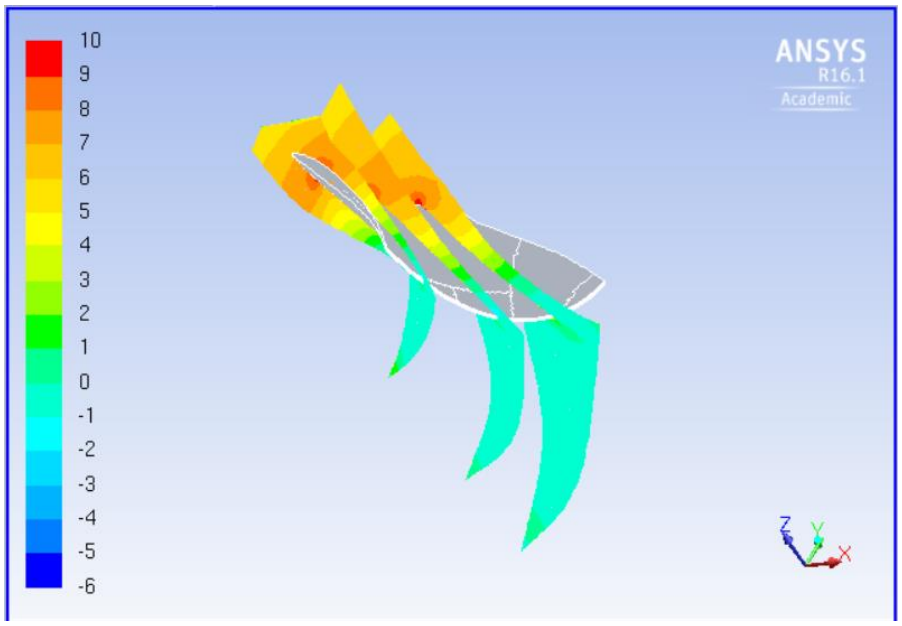

Figure 5-5. Contours of tangential velocity (m/s) for a single Francis GAMM runner blade under high flow conditions with jet 1 injection of 1% volume flow rate.

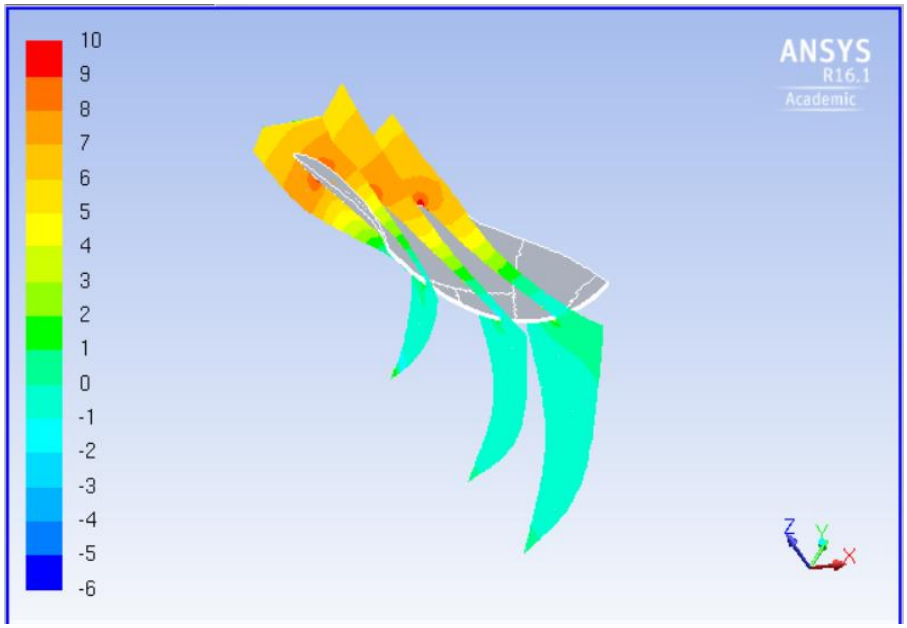

Figure 5-6. Contours of tangential velocity (m/s) for a single Francis GAMM runner blade under high flow conditions with jet 1 injection of 2% volume flow rate.

A closer inspection of the trailing edge of the runner blade further confirms that the water jet injection technique is turning the bulk mean flow. Figures 5-7 to 5-9 demonstrate that activating a jet on one side of the runner blade effectively turns the flow towards the opposite side

of the runner blade. All of the figures show the relative velocity vectors in the same plane from the same viewpoint. Note that the trailing edge of the runner blade resides at the top of the view, and the right-hand side is the figure is the suction side of the runner blade. Since Figures 5-7 to 5-9 show the relative velocity of the flow, the figures show only the change of the flow with respect to the runner blades. Absolute velocity vectors could be derived by adding the tip velocity to these vectors. In Figure 5-7, no jets are activated and therefore the relative velocity vectors, as expected, are roughly parallel with the trailing edge of the runner blade. In Figure 5-8, Jet 1 is activated and the flow is turned towards the suction side of the blade. Similarly, Figure 5-9 shows that the activation of Jet 2 turns the flow towards the pressure side of the runner blade. These results are in agreement with the change in tangential flow discussed above.

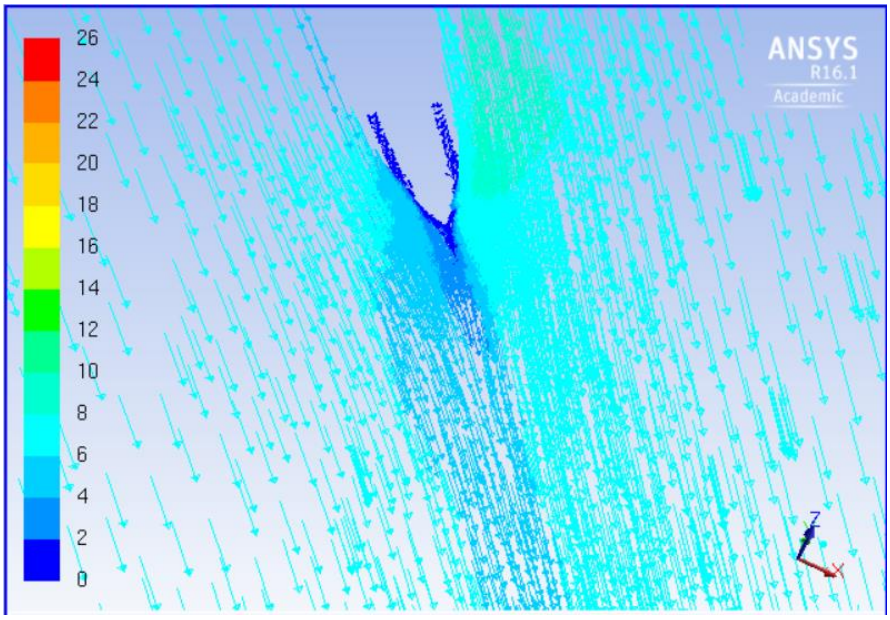

Figure 5-7. Relative velocity vectors (m/s) in a single plane for a single Francis GAMM runner blade under high flow conditions no water jet injection.

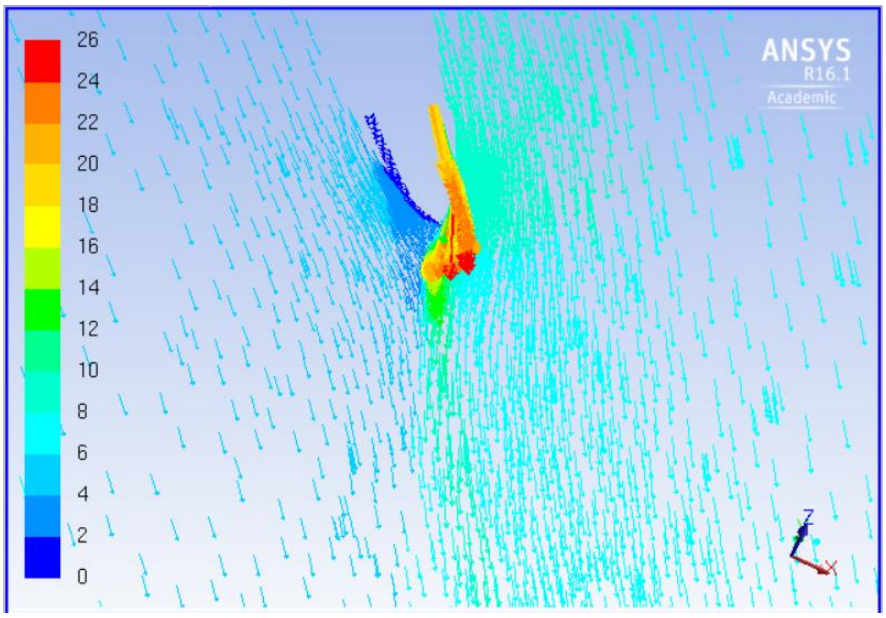

Figure 5-8. Relative velocity vectors (m/s) in a single plane for a single Francis GAMM runner blade under high flow conditions with jet 1 injection of 2% volume flow rate.

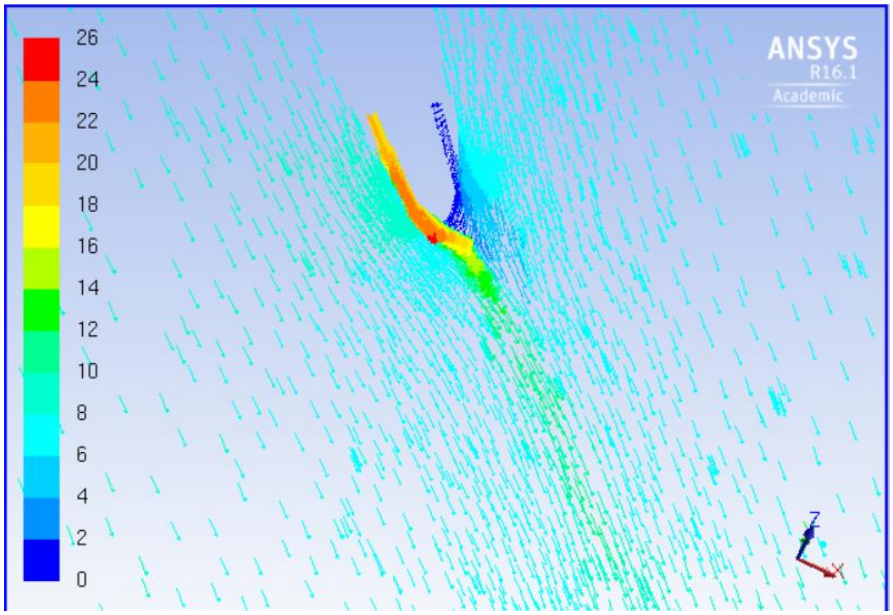

Figure 5-9. Relative velocity vectors (m/s) in a single plane for a single Francis GAMM runner blade under high flow conditions with jet 2 injection of 2% volume flow rate.

The model was used to simulate low flow conditions in conjunction with water jet application as well. Unlike the high flow case, blowing from Jet 2 resulted in an increase of

efficiency for the hydroturbine. This is likely a direct result of the lessening of the residual tangential velocity that occurred as a consequence of the water jet injection. Despite the fact that the head increased when the jets were turned on, the increase in torque was enough to produce a net increase in efficiency. Thus, it is proposed that future work involve low flow off-design cases only.

Table 5-2. Comparison of the computed head, H, torque T and efficiency η for the low flow conditions with various types of blowing

Data Source	H (m)	T (Nm)	η (%)
No blowing	3.88	188	89.5
1% Jet 2 Blowing	4.00	195	89.9
2% Jet 2 Blowing	4.24	207	90.3
3% Jet 2 Blowing	4.51	219	89.9

Figures 5-10 to 5-12 demonstrate that water jet injection effectively lessens the presence of residual swirl. Without water jet injection, the low flow conditions displayed in Figure 5-10 show that the residual tangential velocity after the trailing edge is largely positive, especially in the upper contour plots. This was predicted because low flow conditions result in a residual tangential velocity in the same direction as the tip velocity. As the blade is rotating in a counterclockwise direction, this residual tangential velocity is seen as expected. Furthermore, water jet injection from Jet 2 changes the mean flow towards a direction opposite runner blade rotation (*Chapter 3*). Figure 5-11 shows that the positive tangential velocity has significantly decreased when Jet 2 is injecting water. In Figure 5-12, most of the positive residual velocity has been decreased to a point such that much tangential velocity past the trailing edge is negative. Thus, water injection from Jet 2 has effectively changed the direction of the mean bulk flow in the low flow case.

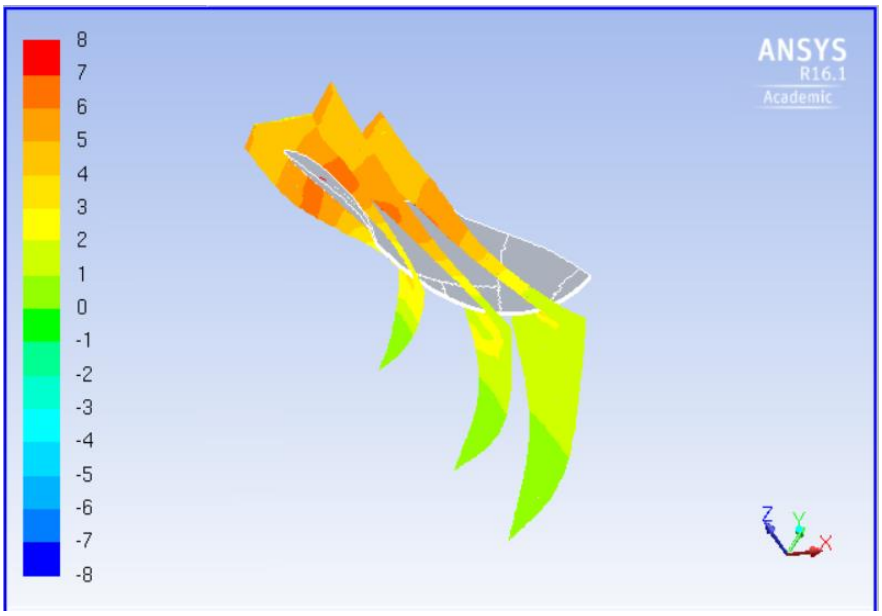

Figure 5-10. Contours of tangential velocity (m/s) for a single Francis GAMM runner blade under low flow conditions with no water jet injection.

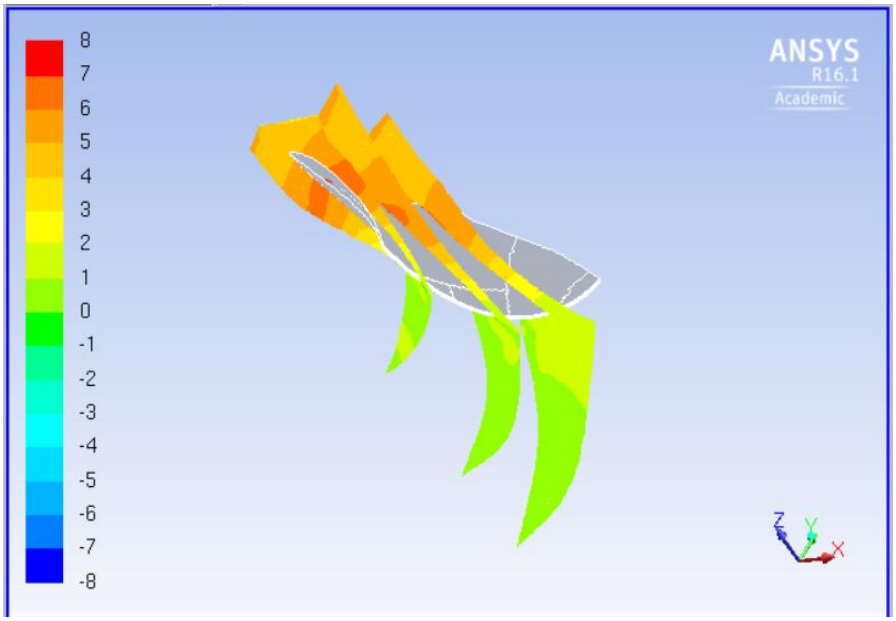

Figure 5-11. Contours of tangential velocity (m/s) for a single Francis GAMM runner blade under low flow conditions with jet 2 injection of 2% volume flow rate.

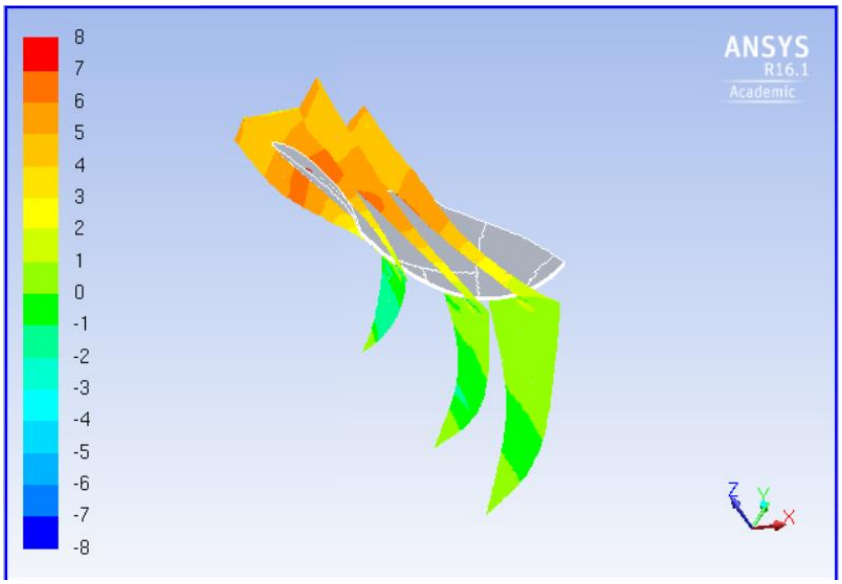

Figure 5-12. Contours of tangential velocity (m/s) for a single Francis GAMM runner blade under low flow conditions with jet 2 injection of 3% volume flow rate.

Identically to the high flow case, a closer inspection of the trailing edge of the runner blade further confirms that the water jet injection technique is turning the bulk mean flow. Figures 5-13 and 5-14 demonstrate that activating jet 2 (on the suction side of the runner blade) effectively turns the flow towards the pressure side of the runner blade. Both of the figures show the relative velocity vectors in the same plane from the same viewpoint. Note that the trailing edge of the runner blade resides at the top of the view, and the right-hand side is the figure is the suction side of the runner blade. Just as with the high flow case, since Figures 5-13 to 5-14 show the relative velocity of the flow, the figures show only the change of the flow with respect to the runner blades. Absolute velocity vectors could be derived by adding the tip velocity to these vectors. In Figure 5-13, no jets are activated and therefore the relative velocity vectors, as expected, are roughly parallel with the trailing edge of the runner blade. In Figure 5-14, Jet 2 is activated and the flow is turned towards the pressure side of the blade. This is in agreement with the change in tangential flow discussed above.

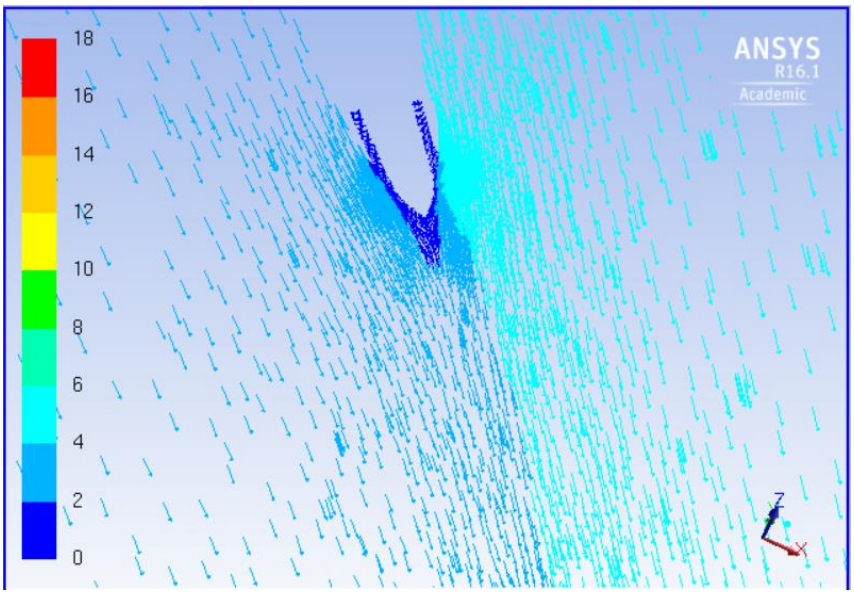

Figure 5-13. Relative velocity vectors (m/s) in a single plane for a single Francis GAMM runner blade under high flow conditions with no water jet injection.

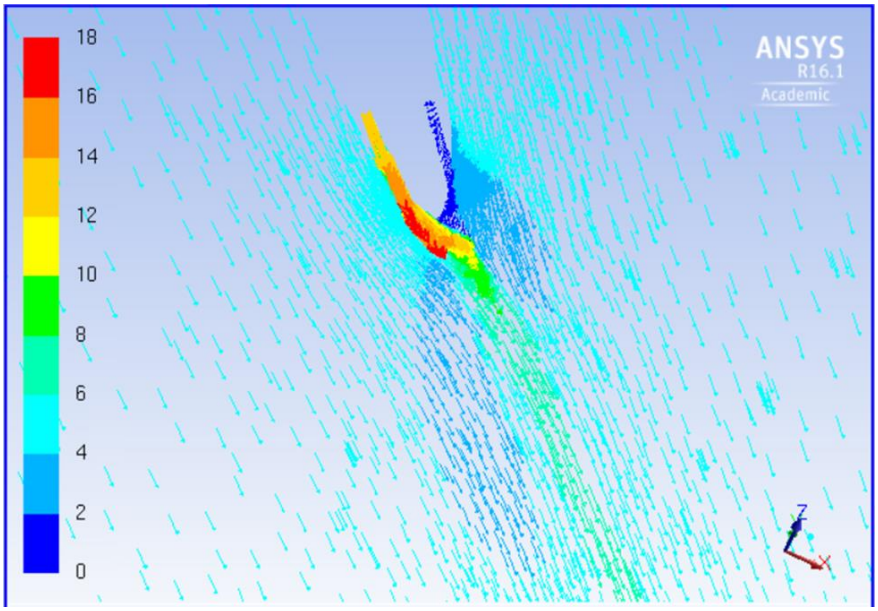

Figure 5-14. Relative velocity vectors (m/s) in a single plane for a single Francis GAMM runner blade under low flow conditions with jet 2 injection of 2% volume flow rate.

Chapter 6

Conclusions and Future Work

The present work determined that water jet injection through the trailing edge of the runner blade did not increase the off-design efficiency under high flow conditions and was unlikely to increase the off-design efficiency in the low flow case. Although the water jet injection did slightly increase the off-design efficiency under low flow conditions, this gain is offset for two reasons. Firstly, the energy needed to pump the water jets has not been calculated or subtracted from the overall efficiency. It is therefore probable than the additional power needed would result in a net loss of efficiency despite the improved hydroturbine performance. Furthermore, the increase in efficiency requires a larger operational net head. If this head were available, it is likely that the hydroturbine operators would be operating at that condition instead. Thus, it is likely that this method would be used only in special circumstances in which the hydroturbine was operating at a lower head than was available, perhaps due to environmental concerns or regulations. Regardless of any gain in efficiency, the ability to change the swirl and prevent the formation of a vortex rope may be beneficial in low flow cases since the unsteady vortex rope can produce a substantial amount of vibration.

Additionally, the model had several limitations in real world application. The curvature of the runner blades would make the manufacturing of the jet channels very difficult to implement, although perhaps not for modern addictive manufacturing techniques (3-D printing). However, there are some hydroturbine design companies that inject air from the trailing edges of the runner blades. Implementing their design with water instead of air (which was for aerating purposes) may be able to achieve a similar change in residual swirl as reported here.

In addition, it is proposed that the slots be broken up into several independent regions. Since the runner blades are twisted, it could be possible for certain sections to be working against the elimination of residual swirl. Independent water jet sections could resolve this problem by injecting water only from the appropriate sections as needed.

Bibliography

[1] Y. A. Cengel and J. M. Cimbala. *Fluid Mechanics: Fundamentals and Applications*. McGraw Hill, New York, third edition, 2013.

[2] H. Nilsson and L. Davidson. Validations of CFD against detailed velocity and pressure measurements in water turbine runner flow. *Int. J. Numer. Meth. Fluids*, 41, 200

[3] B.J. Lewis. Improving Unsteady HYdroturbine Performance During Off-design Operation by Injecting Water from the Trailing Edge of the Wicket Gates. (Doctoral Dissertation), *The Pennsylvania State University*, 2014.

[4] C. E. Brennen. *Cavitation and Bubble Dynamics*. Oxford University Press, Online: http://authors.library.caltech.edu/25017/4/chap7.htm, 1995.

[5] G. Sottas and I. L. Ryhming. *3D-Computation of Incompressible Internal Flows. Proceedings of the GAMM Workshop held at EPFL, 13-15 September 1989, Lausanne, Switzerland*. Notes on Numerical Fluid Mechanics, Volume 39. Vieweg, Braunschweig/Wiesbaden, 1989.

Appendix

Images of Computational Model

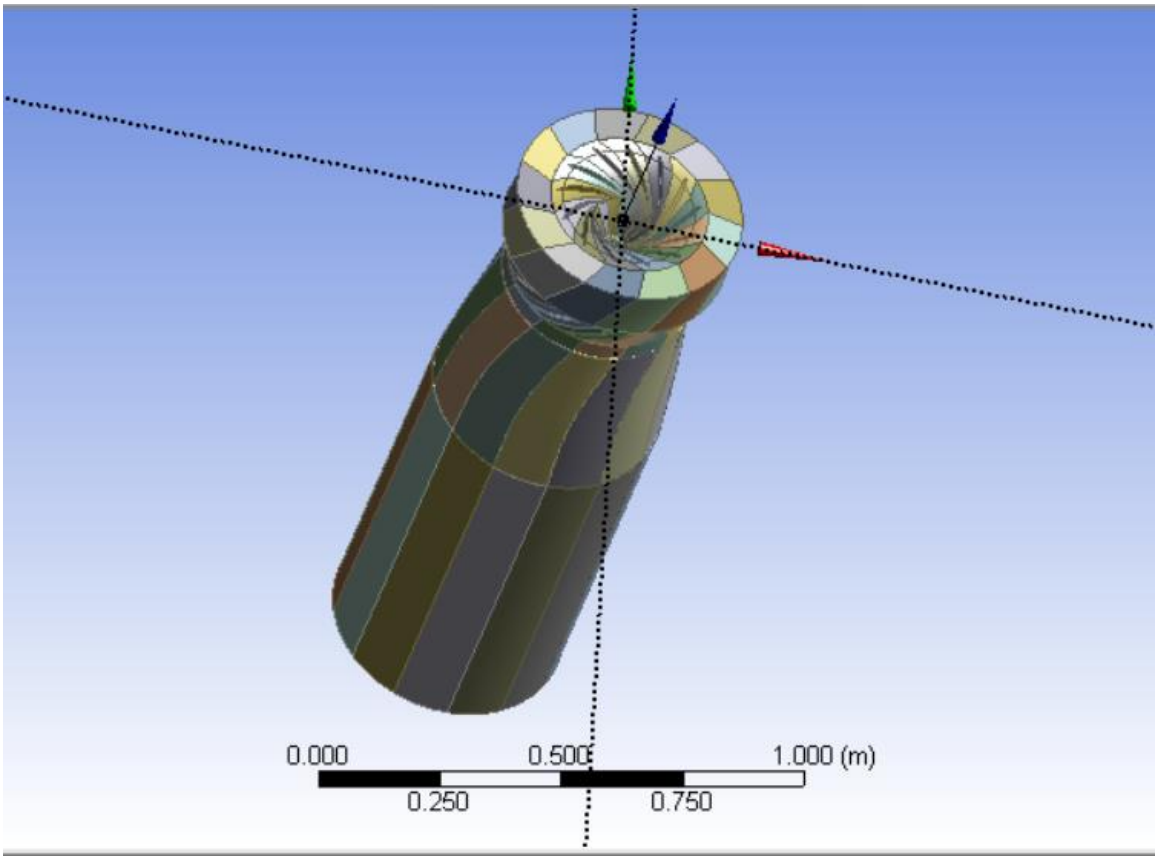

Figure A-1. Geometry of full-wheel hydroturbine model (including added extension past the draft tube) as it could be modeled in ANSYS-Fluent. (Blue arrow is the z direction)

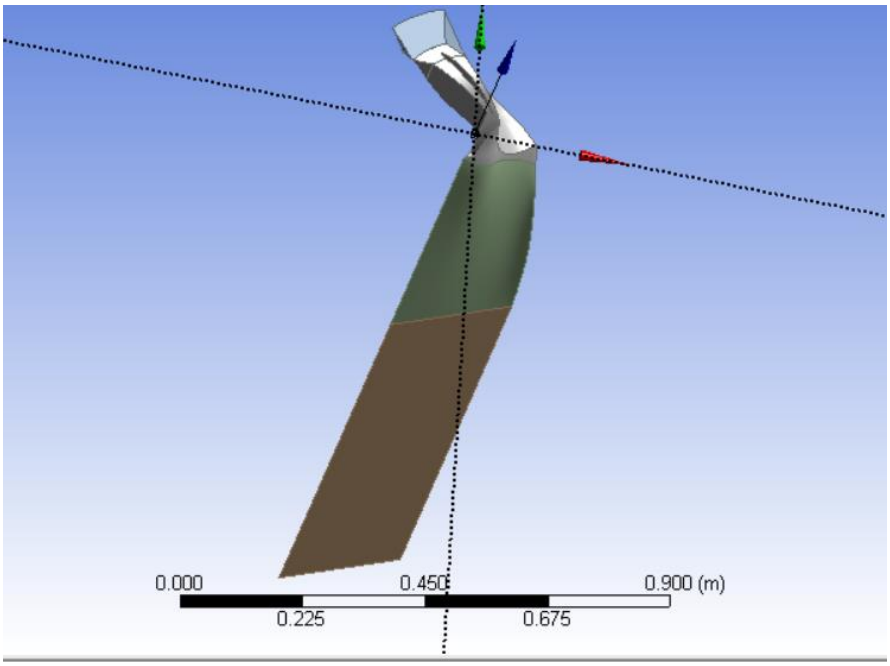

Figure A-2. Actual computational domain for the model. Note that this is just a periodic slice of the full-wheel model above

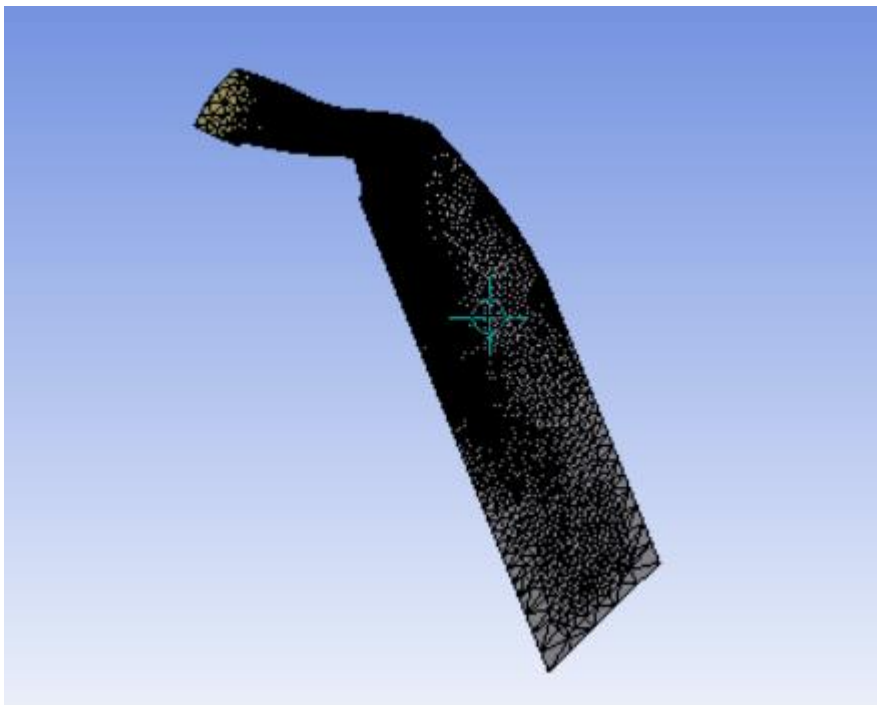

Figure A-3. Mesh of the computational model (3.67 million cells)

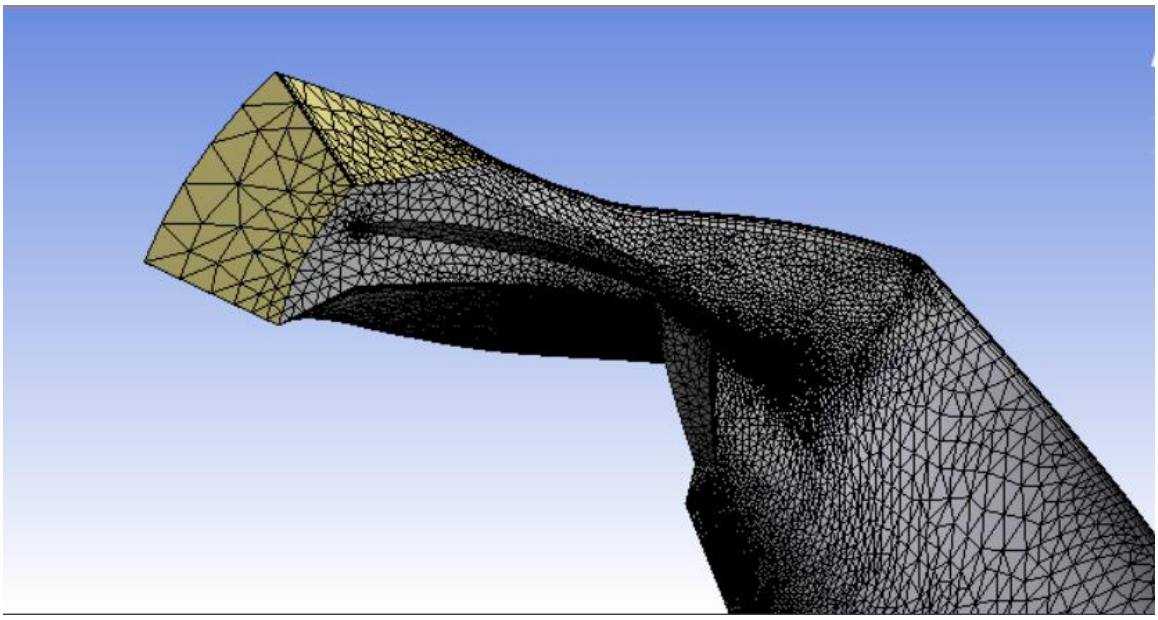

Figure A-4. Close up of the computational mesh in the region of the runner blade. Note the increased mesh count in the region surrounding the trailing edge.